GSK3 is a metabolic checkpoint regulator in B cells

Julia Jellusova[1,2], **Matthew H. Cato**[1,2], **John R. Apgar**[1,2], **Parham Ramezani-Rad**[1,2], **Charlotte Leung**[1,2], **Cindi Chen**[1,2], **Adam D. Richardson**[2], **Elaine M. Conner**[3], **Robert J. Benschop**[3], **James R. Woodgett**[4], and **Robert C. Rickert**[1,2]

[1]Tumor Microenvironment and Cancer Immunology Program, Sanford Burnham Prebys Medical Discovery Institute, La Jolla, CA, 92037, USA

[2]NCI-designated Cancer Center, Sanford Burnham Prebys Medical Discovery Institute, La Jolla, CA, 92037, USA

[3]Eli Lilly & Company

[4]Lunenfeld-Tanenbaum Research Institute, Mount Sinai Hospital, Toronto, ON, M5G 1X5, Canada and Department of Medical Biophysics, University of Toronto, Toronto, M5G 2M9, ON, Canada

Abstract

B cells predominate in a quiescent state until antigen is encountered, which results in rapid growth, proliferation and differentiation. These distinct cell states are likely accompanied by differing metabolic needs, yet little is known about the metabolic control of B cell fate. Here we show that glycogen synthase kinase 3 (GSK3) is a metabolic sensor that promotes the survival of naïve recirculating B cells by restricting cell mass accumulation. In antigen-driven responses, GSK3 was selectively required for CD40-mediated regulation of B cell size, mitochondria biogenesis, glycolysis and reactive oxygen species (ROS) production. GSK3 was required to prevent metabolic collapse and ROS-induced apoptosis when glucose became limiting, functioning in part by repressing c-Myc-dependent growth. Importantly, we found that GSK3 was required for the generation and maintenance of germinal center B cells, which require high glycolytic activity to support growth and proliferation in a hypoxic microenvironment.

Introduction

B cell responses are initiated by antigen uptake and presentation to CD4^{+} T cells, which in turn co-stimulate B cells via CD40 engagement and provision of interleukins (IL)[1]. Some of these antigen-experienced B cells undergo further differentiation in the germinal center (GC), which is a unique microenvironment that coordinates antigen-driven clonal selection of B cells. B cells proliferate and undergo somatic hypermutation in the histologically distinct "dark zone" of the GC and subsequently migrate to the "light zone" to bind antigen retained by resident follicular dendritic cells and receive pro-survival and differentiative cues from follicular helper T cells[1]. While B cells in the dark zone express genes associated with cell division, B cells in the light zone exhibit genetic signatures associated with B cell antigen receptor (BCR) and CD40 stimulation as well as c-Myc activity. The signaling events that mediate selection in the GC are poorly understood and, as illustrated by c-Myc expression[2, 3], likely apply to a small and temporally restricted fraction of B cells.

While resting lymphocytes have low metabolic requirements, activated cells face increased energetic and biosynthetic demands to support cell growth, proliferation and effector function. In B cells, enhanced glycolytic activity has been observed after BCR, CD40 or IL-4 stimulation[4, 5, 6]. The phosphatidylinositol-3-OH kinase (PI(3)K) signaling pathway has been implicated in regulating glucose catabolism after BCR stimulation[4], but appears to be dispensable for IL-4 mediated glucose utilization[6]. However, an understanding of many fundamental aspects of metabolic regulation in B cells is lacking. Specifically, it is unclear how B cell metabolism is maintained in the quiescent state; how cytokine- and BCR-induced signaling impact metabolic reprogramming; and how B cell survival is affected in metabolically challenging situations.

Here, we identify glycogen synthase kinase 3 (GSK3) as a metabolic sensor that integrates cytokine-induced cell growth and proliferation with nutrient availability. GSK3 is a ubiquitously expressed kinase with more than 50 known targets that can strongly impact cell differentiation, proliferation, survival and transformation[78, 9]. It is expressed in α and β isoforms that are highly homologous and exhibit similar substrate specificities. Notably, GSK3 is constitutively active in resting and nutrient-deprived cells, but is disabled by phosphorylation-dependent degradation upon stimulation[10]. This phosphorylation event on S9 or S21 can be mediated by many kinases such as PKA[11], Akt[10], p70S6K[12] and PKC[13]. There is also evidence that GSK3 activity promotes distinct outcomes depending upon the cell type and the impact of other signaling events[14].

Relatively little is known about the role of GSK3 in lymphocytes, perhaps owing to the redundant functions of the α and β isoforms. In a previous study, we showed that GSK3β is inactivated in a PKA-dependent manner in GC B cells, allowing for the accumulation of cyclin D3 and promoting proliferative expansion[15]. Here, we show that GSK3 restrains cell mass accumulation in resting B cells, as well as B cell growth, metabolic activity and proliferation. This effect is most prominent upon CD40–IL-4 co-stimulation, suggesting that GSK3 limits responses to T cell help. However, GSK3 also attenuates ROS production to maintain the redox state and prevent apoptosis. These opposing roles of GSK3 are critical for the regulation of the GC reaction.

Results

GC B cells face increased metabolic demands

Since GC B cells are under strong proliferative stress, we posited that they would have increased energy and nutrient demands to fuel biosynthesis. Indeed, we found that murine GC B cells are larger (Fig. 1a) with increased protein content (Fig. 1b), enhanced glucose uptake (Fig. 1c) and increased mitochondrial content (Fig. 1d) relative to follicular B cells. Since the GC microenvironment arises as a poorly vascularized site of intense cell proliferation, we also reasoned that it may be oxygen limited. In fact, injection of mice with pimonidazole, which forms thiol-containing protein adducts in hypoxic cells, selectively identified large areas within GCs (Fig. 1e). Correspondingly, GC B cells selectively expressed the transcription factor hypoxia-inducible factor-1α (HIF-1α), which drives the expression of several glycolytic genes (Fig. 1f)[16]. Consistent with increased glucose uptake, inhibition of glycolysis with the hexokinase inhibitor 2-deoxy-D-glucose (2-DG) resulted in a significant decrease in the percentage of GC B cells (Fig. 1g), whereas the overall percentage of B cells, the ratio of $CD4^+:CD8^+$ cells and the percentage of follicular helper T ($CD4^+$, $PD1^+$) cells was not significantly altered (Supplementary Fig. 1a-c). Thus, glycolysis is an important feature of GC B cells, supporting anabolism in a hypoxic microenvironment.

Profiling BCR and metabolic signaling in the GC

Signaling events that determine the individual fates of B cells within the GC are poorly understood. To interrogate GC B cell signaling, we performed mass cytometric analysis of intracellular effectors associated with BCR activation and metabolism. GSK3 was of central interest because of its presumptive role in GC B cell growth, proliferation and survival through the regulation of c-Myc, cyclin D3 and Mcl-1 stability, respectively[17]. In addition to assessing GSK3 inactivation (phospho-GSK3 S9/S21), we also examined the abundance of c-Myc and Bcl-6, which regulate the transcription of numerous metabolic genes. Enhanced protein synthesis driven by the mammalian target of rapamycin complex 1 (mTORC1) pathway was measured by phosphorylation of S6 ribosomal protein (phospho-S6 S235/ S236). To assess BCR signaling, phosphorylation of PLC-γ2 (Y759), BLNK (Y84) and Erk (T202/Y204) was measured. For reference, anti-IgM induced signaling was examined in marginal zone B cells (Supplementary Fig. 1d). The viSNE algorithm was used to identify cells in the GC that showed similar signaling profiles[18]. As expected, PLC-γ and BLNK identified a similar fraction of GC B cells (Fig. 1h). Whilst Bcl-6 was expressed by most GC B cells, c-Myc was mainly expressed by cells signaling via the PLC-γ–BLNK pathway (Fig. 1h). GSK3 inactivation and consequent β-catenin accumulation was found in a large fraction of GC B cells that encompassed BCR-activated cells (Fig. 1h and Supplementary Fig. 1e). Although GSK3 has been reported to regulate both c-Myc accumulation and mTOR signaling and thus S6 phosphorylation, S6 phosphorylation was confined to a small subpopulation of GC B cells that was also positive for IgG1 (Fig. 1h). Moreover, high amounts of c-Myc and phosphorylated S6 were found in distinct subsets of GC B cells, suggesting that mTOR- and c-Myc-dependent signaling pathways may act in parallel to regulate cell metabolism in the GC.

GSK3 promotes B cell quiescence and homeostasis

To directly address GSK3 function in the regulation of B cell homeostasis and function, we intercrossed mice harboring *lox*P-flanked *Gsk3a* or *Gsk3b* alleles (*Gsk3a*[L/L], *Gsk3b*[L/L])[19] with *Cd19*[Cre] mice[20]. *Cd19*[Cre]*Gsk3a*[L/L]*Gsk3b*[L/L] mice (hereafter referred to as *Cd19*[Cre]*Gsk3ab*[L/L]) showed significantly decreased relative and total B cell numbers in the spleen (Fig. 2a and Supplementary Fig. 2a) and lymph nodes (Fig. 2b and Supplementary Fig. 2b), but normal follicular architecture in the spleen (Supplementary Fig. 2c). Decreased B cell numbers can result from defective B cell generation, maturation or survival. As *Cd19*[Cre]-mediated deletion is incomplete in early B cell development[20], we did not anticipate defects in B cell development. Consistently, pro-B (B220^{+}CD43^{+}BP1^{−}), large pre-B (B220^{+}CD43^{+}BP1^{+}), small pre-B (B220^{+}CD43^{−}IgM^{−}), and immature B (B220^{lo}CD43^{−}IgM^{+}) cells were present in *Cd19*[Cre]*Gsk3ab*[L/L] mice at similar frequencies as control mice (Supplementary Fig. 2d). By contrast, the frequency of recirculating mature (B220^{hi}CD43^{−}IgM^{+}) B cells was significantly decreased in the bone marrow of *Cd19*[Cre]*Gsk3ab*[L/L] mice (Supplementary Fig. 2d). In the spleen, the percentage of mature follicular (B220^{+}CD21^{lo}IgM^{+}) B cells was significantly decreased, and the percentage of transitional T1 (B220^{+}CD21^{−}IgM^{hi}) cells was slightly increased (Fig. 2c). To determine the efficiency of GSK3 deletion in *Cd19*[Cre]*Gsk3ab*[L/L] B cells, splenic B cell lysates were immunoblotted for GSK3. Little GSK3α or GSK3β protein was detectable in B cells from *Cd19*[Cre]*Gsk3a*[L/L] or *Cd19*[Cre]*Gsk3b*[L/L] mice, respectively (Fig. 2d). However, residual expression of both GSK3 isoforms was detected in cell lysates from *Cd19*[Cre]*Gsk3ab*[L/L] mice (Fig. 2d), suggesting a selective advantage for B cells that maintain GSK3 expression. Moreover, GSK3-deficient B cells also downregulated IgD (Supplementary Fig. 2e) and exhibited significant increases in cell size (Fig. 2e), protein content (Fig. 2f) and glucose consumption (Fig. 2g), suggesting that GSK3 may be required for B cells to persist in a quiescent state.

To better assess the acute role of GSK3 in the survival of mature B cells, we employed hCd20-Tam[Cre] mice that inducibly activate Cre in mature B cells[21], resulting in efficient loss of GSK3 protein following tamoxifen treatment (Fig. 2h). These mice also expressed the Rosa26-flox-STOP-YFP[22] transgene to identify cells that have experienced Cre as YFP[+]. By comparing the decline in the percentage of YFP^{+} cells in hCd20-Tam[Cre] (Ctrl) and hCd20-Tam[Cre] Gsk3ab[L/L] (dKO) mice after tamoxifen treatment, the turnover of mature GSK3-deficient B cells could be assessed. In control mice, the percentage of YFP[+] follicular B cells in the spleen on days 26 and 47 post-induction was ~77% and 60% (Fig. 2i), which is consistent with the expected half-life of mature B cells[23]. By contrast, the percentage of YFP[+] follicular B cells was ~35% and ~13% on days 26 and 47, respectively, in hCd20-Tam[Cre] Gsk3ab[L/L] mice (Fig. 2i). While the frequency of YFP[+] marginal zone B cells, which are known to be long-lived, did not decrease significantly in wild-type mice over the course of the experiment, the population of YFP[+] marginal zone B cells in hCd20-Tam[Cre] Gsk3ab[L/L] mice was significantly decreased (Supplementary Fig. 2f). These findings indicate that GSK3 is needed for the survival of both follicular and marginal zone B cells.

The IgM–IgD profile of GSK3-deficient B cells was normal early after GSK3 ablation, but IgD was significantly down-regulated at later time points (data not shown). Thus, low IgD

expression on GSK3-deficient B cells is not due to impaired B cell maturation, but may reflect a perturbed quiescent state. To evaluate the impact of acute versus developmental loss of GSK3, spontaneous cell mass accumulation was measured after induced GSK3 ablation in mature B cells. We found that the acute loss of GSK3 caused a slow accumulation of cell mass (Fig. 2j). *hCd20*-Tam[Cre] *Gsk3ab*[L/L] B cells were comparable in size to control B cells 1 day after tamoxifen-induced GSK3 deletion, but slowly increased in size and were significantly larger than control B cells by day 14 (Fig. 2j). Thus, GSK3 controls the metabolic state and long-term survival of mature resting B cells.

GSK3 is required for T cell-dependent B cell responses

Previously, we have shown that GSK3β is phosphorylated on the inhibitory residue S9 in GC B cells[15]. Therefore, to determine the role of GSK3 in the GC response, we immunized *hCd20*-Tam[Cre] *Gsk3ab*[L/L] mice with the T cell-dependent antigen, sheep red blood cells (SRBCs). *hCd20*-Tam[Cre] *Gsk3ab*[L/L] mice displayed an impaired immune response, as indicated by significantly reduced antigen-specific IgG1 and IgM titers (Fig. 3a), slightly decreased percentage of plasma cells (Fig. 3b) and a significant reduction in the GC B cell compartment (Fig. 3c,d). Since the GC is the site of antibody affinity maturation, we performed additional immunizations with 4-Hydroxy-3-nitrophenyl acetyl (NP) Keyhole Limpet Hemocyanin (KLH) with a conjugation ratio of 25:1 (NP_{25}) and measured titers of high (NP_4) and low (NP_{23}) affinity antigen-specific serum IgG and IgM. In contrast with control animals, *hCd20-Tam*[cre]*Gsk3ab*[L/L] mice showed poor production of both high- and low-affinity antigen-specific antibodies (Fig. 3e). These data demonstrate that GSK3 is required in B cells for humoral responses to T cell-dependent antigens.

GSK3 inhibits CD40-induced B cell proliferation

To determine if naïve GSK3-deficient B cells are capable of differentiating into "induced GC B cells"[24], we used a fibroblast feeder layer expressing membrane-bound CD40-ligand and secreted BAFF in the presence of exogenous IL-4. We found that GSK3-deficient B cells efficiently acquired a GC phenotype, as indicated by upregulating Fas and GL7 (Fig. 4a). To analyze proliferation to individual and combined stimuli, we cultured B cells with anti-CD40 alone, anti-CD40+IL-4, anti-IgM or lipopolysaccharide (LPS). GSK3-deficient B cells stimulated with anti-CD40 alone or with anti-CD40+IL-4 showed increased proliferation (Fig. 4b,c and Supplementary Fig. 3a); however, anti-IgM- or LPS-induced proliferation was normal (Fig. 4b,c). Since B cells can be exposed to multiple stimuli in the GC, we mimicked these events by first stimulating GSK3-deficient and control B cells with anti-IgM for 16 h and then added anti-CD40, IL-4 and BAFF for an additional three days. GSK3-deficient B cells cultured under these conditions displayed increased proliferation in comparison to wild-type cells (Supplementary Fig. 3b), suggesting that GSK3 limits CD40-mediated proliferation in the context of other stimuli.

To confirm that the increase in CD40-mediated proliferation observed *in vitro* reflects the properties of GSK3-deficient B cells *in vivo*, we administered agonistic CD40 antibody by i.p. injection into *Cd19*[Cre]*Gsk3ab*[L/L] and control mice and measured B cell proliferation by BrdU incorporation 3 days later. In agreement with the *in vitro* results, GSK3-deficient B

cells exhibited enhanced BrdU incorporation after *in vivo* anti-CD40 administration (Fig. 4d). In summary, our results indicate that GSK3 limits CD40-mediated proliferation.

GSK3 limits CD40-induced metabolic activity

To assess the role of GSK3 in the regulation of B cell growth and metabolism, B cells were isolated from *hCd20*-Tam[Cre] *Gsk3ab*[L/L] mice 7 days after tamoxifen treatment. At this timepoint, GSK3-deficient B cells are comparable in cell size to unstimulated control B cells. After anti-IgM stimulation, the size of both GSK3-deficient and control B cells increased similarly (Fig. 4e), indicating that GSK3 does not regulate cell growth after anti-IgM stimulation. By contrast, anti-CD40+IL-4-stimulated GSK3-deficient B cells were significantly larger than control B cells (Fig. 4e). Similarly, anti-IgM+CD40+IL4+BAFF-stimulated GSK3-deficient B cells were slightly larger than wild-type B cells (Supplementary Fig. 3c). To determine if glucose is differentially catabolized in normal versus GSK3-deficient B cells, we measured glucose consumption and lactate production *in vitro*. Unstimulated B cells showed little metabolic activity, but glucose consumption by both control and GSK3-deficient B cells increased after anti-IgM stimulation (Fig. 5a). However, anti-IgM stimulated GSK3-deficient B cells produced lower amounts of lactate (Fig. 5a). By contrast, anti-CD40+IL-4-stimulated GSK3-deficient B cells exhibited increased lactate production and glucose consumption compared to control B cells (Fig. 5a). Interestingly, although the average number of cell divisions of CD40+IL-4-stimulated and anti-IgM stimulated B cells was comparable (1.1 vs 1.4, Fig. 4c), anti-CD40+IL-4-stimulated GSK3-deficient B cells produced more lactate than IgM stimulated cells (Fig. 5a). This finding suggests that increased lactate production in anti-CD40+IL-4 stimulated GSK3-deficient B cells is not simply a byproduct of increased proliferation. However, to exclude the contribution of accelerated proliferation to increased metabolic activity in GSK3-deficient B cells, we used Seahorse XF technology to analyze oxidative phosphorylation and glycolysis in real time. Oxygen consumption (OCR) was used as a measurement of oxidative phosphorylation, and extracellular acidification (ECAR) as a measurement of glycolysis. After measuring basal respiration, cells were treated with oligomycin to block ATP production, followed by FCCP (carbonyl cyanide 4-(trifluoromethoxy) phenylhydrazone) to induce maximal oxygen consumption and Rotenone + Antimycin to inhibit the electron transport chain. Both basal and maximal respiration were increased in anti-CD40+IL-4 stimulated GSK3-deficient B cells versus wild-type counterparts (Fig. 5b,c). Inhibition of ATP generation from respiration causes an increase in the rate of glycolysis to supply cells with energy. Both anti-CD40+IL-4-stimulated GSK3-deficient and control B cells showed an increase in ECAR after oligomycin inhibition, but ECAR was slightly higher under all conditions in GSK3-deficient B cells (Fig. 5b,c). Similar experiments were performed with anti-IgM stimulated cells; however, no significant differences were observed between GSK3-deficient and control B cells (Supplementary Fig. 4). These findings suggest that GSK3 limits B cell activation by inhibiting CD40+IL-4-induced metabolic adaptations.

GSK3 promotes rapamycin sensitivity and c-Myc degradation

Our data demonstrate that GSK3 limits cellular growth, metabolic activity and proliferation of anti-CD40+IL-4-stimulated B cells. To determine the biochemical of these findings, we

first focused on the role of mTORC1 as a central regulator of cell metabolism[25]. The mTORC1 inhibitor rapamycin efficiently inhibited anti-CD40+IL-4-mediated proliferation and growth of control B cells, but did not affect the growth and only marginally inhibited proliferation of GSK3-deficient B cells (Fig. 6a-c). In contrast with anti-CD40+IL-4 stimulated cells, anti-IgM stimulated GSK3-deficient B cells showed little proliferation and comparable cell size with control B cells after mTORC1 inhibition (Fig. 6d-f). To determine if mTORC1 activity is enhanced in GSK3-deficient B cells, we measured the abundance of mTORC1-phosphorylated p70S6K (T389), as well as p70S6K-phosphorylated ribosomal protein S6 (S235, S236, S240 and S244) in anti-CD40+IL-4–stimulated B cells (Fig. 6g). Both p70S6K and S6 were phosphorylated in control and GSK3-deficient B cells, and their phosphorylation was abolished upon rapamycin treatment (Fig. 6g). By contrast, the GSK3 target β-catenin was protected from degradation in GSK3-deficient B cells, and was unaffected by rapamycin treatment (Fig. 6g). These findings suggest that GSK3-deficient B cells are able to proliferate and grow independently of S6 phosphorylation, and thus are less sensitive to inhibition of mTORC1.

GSK3 is known to phosphorylate the transcription factor c-Myc, facilitating its degradation[26]. Consistent with this finding, anti-CD40+IL-4-stimulated GSK3-deficient B cells showed increased abundance of c-Myc relative to control and freshly isolated B cells (Fig. 6g and Supplementary Fig.5a,b). c-Myc accumulated to a similar degree in anti-IgM– stimulated GSK3-deficient B cells and control B cells (Fig. 6h and Supplementary Fig.5c), indicating distinct regulation of c-Myc stability downstream of the BCR versus CD40+IL-4. To address whether enhanced c-Myc expression could account for the altered growth of CD40+IL-4–stimulated GSK3-deficient B cells, we compared the effects of Myc overexpression and GSK3 loss in B cells. B cell-specific–transgenic (*Myc*-tg) mice were generated by intercrossing *Rosa26Stop*[FL]*Myc*[27] and *Cd19*[Cre] mice. In contrast to control B cells, naïve *Myc*-tg B cells expressed substantial amounts of c-Myc protein (Fig. 7a). Upon B cell activation, c-Myc accumulated in both control and *Myc*-tg B cells (Fig. 7a). However, c-Myc abundance remained higher in stimulated *Myc*-tg B cells than control B cells (Fig. 7a). *Myc*-tg mice showed normal B cell maturation (Supplementary Fig. 6); however, the cells were significantly larger, indicating that *Myc* expression is sufficient to induce accumulation of cell mass in unstimulated mature B cells (Fig. 7b). Increased c-Myc was also associated with enhanced proliferation and cell size in response to anti-CD40+IL-4 or, to a lesser extent, anti-IgM stimulation (Fig. 7c,d). Thus, elevated c-Myc expression functionally correlates with the selective responsiveness of GSK3-deficient B cells to anti-CD40+IL-4 stimulation.

c-Myc is known to drive a transcriptional program that promotes glycolysis[28]. Indeed, *Myc*-tg B cells showed increased lactate production after stimulation with anti-CD40+IL-4 or anti-IgM (Fig. 7e). Since most of the c-Myc-positive cells in the GC do not show S6 phosphorylation (Fig. 1h), we sought to determine whether c-Myc can induce proliferation independently of mTORC1 signaling. To this end, we treated anti-CD40+IL4 and anti-IgM stimulated B cells with rapamycin, which inhibited cell division in both anti-IgM and anti-CD40+IL4-stimulated wild-type and *Myc*-tg B cells (Fig. 7f). Thus, unlike GSK3-deficient B cells (Fig. 6), *Myc*-tg B cells remain sensitive to mTORC1 inhibition.

GSK3 promotes B cell survival under glucose restriction

Although GSK3-deficient B cells showed increased metabolism, growth and proliferation *in vitro*, they failed to mount an efficient T cell-dependent immune response *in vivo*. To help resolve this enigma, we analyzed the survival of GSK3-deficient B cells stimulated with IL-4, anti-CD40, anti-CD40+IL-4, anti-IgM, LPS or BAFF. GSK3-deficient B cells displayed normal survival properties in response to each cytokine, except IL-4 (Fig. 8a). However, this defect could be rescued by the addition of anti-CD40. To assess the role of GSK3 in GC B cell survival independent from its function in initiation of the GC response, we immunized *hCd20*-Tam[Cre] *Gsk3ab*[L/L] mice with SRBCs and administered tamoxifen on days 5–7 post-immunization. Fewer GC B cells were recovered from *hCd20*-Tam[Cre] *Gsk3ab*[L/L] mice (Fig. 8b), and Annexin V staining revealed an increased frequency of apoptosis in GSK3-deficient GC B cells (Fig. 8c). However, deletion of *Gsk3* during an ongoing immune response promoted GC B cell proliferation (Fig.8d). Together, these data suggest that *Gsk3* deletion leads to a proliferative burst of GC B cells, but is offset by increased apoptosis.

To explain why GSK3-deficient B cells exhibited differential susceptibility to apoptosis under *in vitro* versus *in vivo* growth conditions, we hypothesized that B cells are cultured in nutrient-rich medium, whereas the GC microenvironment may be nutrient-limited. To analyze the survival of GSK3-deficient B cells under nutrient-stressed conditions, anti-CD40+IL-4-stimulated cells were cultured in glucose-free medium. Whereas GSK3-deficient B cells had normal viability in the presence of glucose, viability was significantly reduced in glucose-free medium (Fig. 8e). Cells respond to metabolic stress by limiting mTORC1 signaling, and inhibition of mTORC1 can improve cell survival under glucose starvation. Correspondingly, rapamycin significantly increased the survival of both control and GSK3-deficient B cells in glucose-free medium, but the degree of rescue was modest, suggesting that mTORC1-independent pathways also contribute to GSK3-dependent B cell survival (Fig. 8e).

In addition to serving as a source of energy, glucose is also needed in the pentose phosphate pathway that provides cells with NADPH, thus supporting intracellular redox balance. Since GSK3-deficient B cells showed enhanced respiration we hypothesized that GSK3-deficient B cells may accumulate mitochondrial mass, leading to increased production of reactive oxygen species (ROS). Indeed, GSK3-deficient B cells had increased mitochondrial content relative to control B cells when stimulated overnight with anti-CD40+IL-4, but not after anti-IgM stimulation (Fig. 8f,g). Consistent with the known role of c-Myc in supporting mitochondrial biogenesis[28], we found that *Myc*-tg B cells exhibited increased mitochondrial mass after both anti-CD40+IL-4 and anti-IgM stimulation (Fig. 8g,h). Anti-CD40+IL-4-stimulated GSK3-deficient B cells did not show a significant increase in ROS production when cultured in complete medium. However, in glucose-free medium they produced more ROS than control B cells (Fig. 8i). Excessive ROS production can lead to oxidation of macromolecules and ultimately to cell death[29]. Indeed, when the ROS scavenger N-acetyl cysteine (NAC) was added to the cultures, survival of GSK3-deficient B cells in glucose-free medium was significantly enhanced (Fig. 8i). Correspondingly, freshly isolated *Cd19*[Cre]*Gsk3ab*[L/L] B cells accumulated more ROS than control B cells, consistent with their

increased cell size and decreased survival *in vivo* (Fig. 8j). Collectively, these data highlight a critical role for GSK3 in curtailing anabolic growth and promoting cell viability under glucose deprivation.

Discussion

Herein we show that rapid growth and proliferation in the GC occurs in a hypoxic environment and thus is limited in blood-derived oxygen and nutrients; findings that are consistent with two reports that were published during the review of our manuscript[30, 31]. We further demonstrate GC B cells undergo metabolic adaptation by increasing mitochondrial biogenesis, glucose uptake and induction of the HIF-1α-dependent glycolytic program[16]. Indeed, the GC response collapses when glycolysis is halted upon 2-DG administration. These findings are consistent with a recent study showing that B cell-specific deletion of the glucose transporter Glut1 results in decreased numbers of mature B cells and reduced production of high- and low-affinity IgM and IgG antibodies in response to a T cell-dependent antigen[32], indicating that glucose metabolism is crucial for an effective B cell immune response.

GSK3 regulates the stability of a number of effector proteins that we postulated would be of importance to B cell activation and differentiation. Indeed, using an inducible system, we demonstrated a B cell-intrinsic requirement for GSK3 in the humoral response, including initiating and sustaining the GC reaction. Unlike GC B cells, cultured GSK3-deficient follicular B cells showed normal responses to BCR stimulation and LPS, and enhanced proliferation, growth, glycolysis and oxidative phosphorylation in response to T cell derived co-stimuli CD40L and IL-4. However, upon glucose deprivation, GSK3-deficient B cells showed enhanced susceptibility to ROS-induced cell death. Thus, we postulate that GSK3 inactivation by upstream kinases promotes GC B cell growth, metabolic activity and proliferation when nutrients are abundant, whereas sustained GSK3 activity constrains these processes and preserves cell viability when nutrients are scarce.

Limited oxygen and nutrient availability may impose a metabolic checkpoint on GC B cells, preventing excessive proliferation and cell growth while supporting B cell differentiation. Interestingly, transcription factors from the HIF family and c-Myc have complementary roles in effecting metabolic reprograming of tumor cells[33], although HIF has been shown to counter Myc-dependent mitochondrial biogenesis and respiration[34]. By analogy, the synergy of the c-Myc and HIF pathways is also likely to be critical in the GC. We found that GSK3 restrains c-Myc-dependent glycolysis and respiration to regulate catabolism and energy production, and attenuate the cytotoxic effects of ROS production. GSK3 is inhibited in GC B cells engaged in BCR signaling, but it is also inhibited in B cells that are not actively signaling via the BCR, including a small subpopulation of B cells with abundant pS6. These cells may be responding to distinct growth stimuli, such as CD40L and IL-4 provided by cognate follicular helper T cells. In support of this view, this same population is enriched for IgG1-expressing B cells, which is a product of CD40L+IL-4 signaling.

The enhanced presence of c-Myc may partially account for the increased growth, metabolic activity and proliferation of GSK3-deficient B cells. We show that c-Myc was increased in

GSK3-deficient B cells stimulated with anti-CD40+IL-4, and that c-Myc overexpression in GSK3-sufficient B cells leads to increased B cell proliferation and cell growth. On the other hand, anti-IgM–stimulated GSK3-deficient B cells show comparable c-Myc abundance with their wild-type counterparts and display normal rates of proliferation and cell growth. Together, these findings indicate that c-Myc is an important regulatory target of GSK3 downstream of CD40.

In addition to c-Myc, mTORC1 is a central regulator of cell metabolism and its activity is dependent on nutrient availability. GSK3 has been previously shown to phosphorylate tuberous sclerosis complex 2 (TSC2), an inhibitor of mTORC1[35]. This phosphorylation event leads to TSC2 activation and thus inhibition of mTORC1. Accordingly, chemical inhibition of GSK3, or GSK3 knockdown has been shown to enhance mTORC1 signaling[35]. On the other hand, GSK3 has also been shown to promote mTORC1 signaling by facilitating assembly with raptor[36, 37]. We did not find any evidence of augmented mTORC1 signaling in the absence of GSK3, since phosphorylation of S6K and its substrate S6 was unaffected. However, proliferation and growth of GSK3-deficient B cells was largely resistant to rapamycin inhibition, suggesting that GSK3 represses protein synthesis by an S6-independent pathway.

In summary, our data demonstrate a critical role for GSK3 in maintaining the quiescent state of naïve recirculating B cells, and regulating GC B cell growth and proliferation in response to nutrient stress and oxygen debt. This regulation is delimited to CD40L–IL-4 signaling and thus a direct outcome of follicular helper T cell interactions in the GC.

METHODS

Mice

Gsk3a[L/L] and *Gsk3b*[L/L] mice were intercrossed with *Cd19*[Cre] mice. In addition, *Gsk3a*[L/L] and *Gsk3b*[L/L] animals were intercrossed with *hCd20-Tam*[Cre] mice [21] and *rosa26-flox-STOP-YFP* mice [22]. For Cre induction, mice were injected i.p. with 1 mg tamoxifen (Sigma-Aldrich) + 10% ethanol in olive oil on three subsequent days. *Gsk3a*[L/L] x *Gsk3b*[L/L] x *hCd20-Tam*[−] and *Gsk3a*[L/L] x *Gsk3b*[L/L] x *hCd20-Tam*[Cre] mice were used as controls. Controls were injected with tamoxifen the same way as experimental animals.

R26Stop[FL]*Myc* mice were intercrossed with *Cd19*[Cre] mice. Used mice were heterozygous for the *R26Stop*[FL]*Myc* locus. All animals were maintained in the animal facility of the Sanford-Burnham Medical Research Institute (SBMRI). Experiments were carried out in accordance with institutional guidelines and regulations.

Cell sorting

Naïve B cells were obtained by negative sorting using CD43-specific beads (Miltenyi) according to manufacturer instructions. Germinal center B cells and non-germinal center B cells were obtained by negative sorting using biotinylated antibodies (CD43, S7,; CD11c, N418; IgD, 11-26 and CD43, S7; CD11c, N418; GL7, respectively. Antibodies obtained from eBioscience), streptavidin-APC (eBioscience) and anti-APC beads (Miltenyi).

Flow Cytometry and Antibodies

To measure cell surface expression of selected markers, single cell suspensions were prepared and stained according to standard procedures. The following antibody clones were obtained from eBioscience: B220 (RA3-6B2), CD23 (B3B4), CD21 (4E3), IgM (II/41), IgD (11-26), BP-1, CD43 (S7), GL7 (GL-7). The following antibodies were obtained from BD Pharmingen: CD138 (281-2), CD95/Fas (Jo2). PBS + 1% FBS + 0.01% sodium azide was used as flow cytometry buffer. To measure mitochondrial content MitoTracker Red CMXRos (Life Technologies) was used. Cells were stained for 30 min at 37 °C with 60 nM MitoTracker Red CMXRos in complete RPMI medium and washed twice before measurement. Cells were analyzed by flow cytometry and microscopy. To measure protein abundance, cells were stained with eFLuor670 (eBiosciences) for 10 min in PBS at 19–25 °C, washed with complete RPMI medium, resuspended in complete RPMI medium, incubated for 5 min, washed again and resuspended in flow cytometry buffer. To detect ROS cells were stained with 10 μM Carboxy H2DCFDA (Invitrogen Molecular Probes) in 1 ml PBS for 20 min at 37 °C and washed twice before measurement. All data were collected using a FACSCanto Flow Cytometer (BD Biosciences).

CyTOF mass cytometry

Mice were immunized with SRBCs to induce germinal centers. Spleen cells were collected in a small volume of ice-cold DPBS containing 50μM cisplatin to stain dead cells. After 1 minute, a 20-fold volume of lyse/fix buffer (BD Biosciences) was added for 10 min at 37 °C. The cells were stained with surface markers followed by permeabilization in 90% methanol for 30 min at –80 °C. Intracellular markers and secondary antibodies were added for 45 min. DNA was stained using 191/193Ir for 15 min followed by one wash in DPBS and one wash in water. The following antibodies (conjugate, supplier) were used to analyze cell signaling in GC B cells: B220 (176Yb, DVS); β-Catenin (147Sm, DVS); CD19 (149Sm, DVS); FAS (biotin, BD); GL7 (FITC, BD); PLC-γ2 (PE, BD); phospho-Erk $^{T202/Y204}$ (167Er, DVS); phospho-BLNK ^{Y84} (147Sm, BD, conjugation by Eli Lilly and Company); phospho-S6 $^{S235/236}$ (175Lu, DVS); phospho-GSK3β ^{S9} (165Ho, CST, conjugation by Eli Lilly and Company); Bcl6 (153Eu, BD, conjugation by Eli Lilly and Company); anti-FITC (174Yb, DVS), anti-biotin (143Nd, DVS), anti-PE (145Nd, DVS), cisplatin (195Pt, Enzo, conjugation by Eli Lilly and Company).

In vitro cell survival and proliferation

To measure cell proliferation and survival under nutrient rich conditions, cells were cultured in complete RPMI medium: RPMI (Corning Cellgro) + 10% FBS (Sigma LOT 14B279-A, 118383 or HyClone LOT AYM178582) + 1x Penicilin/Streptomycin (Corning) + 1 mM Sodium Pyruvate (Cellgro) + 2 mM GlutaGro (Cellgro) + 1x MEM non-essential amino acids (Cellgro) + 50 μM β-Mercaptoethanol (Gibco). Cell survival and proliferation were determined by analyzing forward/side scatter properties of cells and the dilution of the eFluor670 dye, respectively. To calculate the average number of cell division, geometric mean fluorescence intensities (MFI) for eFluor670 at day 3 of cell culture were determined and $\log_2$ values calculated. The $\log_2$ MFIs substracted from the $\log_2$ MFIs of unstimulated cells gave the number of cell divisions. To analyze survival under glucose free conditions,

cells were cultured in glucose-free RPMI (Gibco)+ 10% FBS (HyClone LOT AYM178582 or AWH19892)) + 1x Penicilin/Streptomycin (Corning) + 1 mM Sodium Pyruvate (Cellgro) + 2 mM GlutaGro (Cellgro) + 1x MEM non-essential amino acids (Cellgro) + 50 μM β-Mercaptoethanol (Gibco). The following stimulations or inhibitors were used as indicated: 10 ng/ml rmBAFF (R&D Systems), 10 ng/ml recombinant protein IL-4 (eBioscience), 5 μg/ml anti-CD40 (eBioscience), 12 μg/ml anti-IgM (Jackson Immuno Research), 10 μg/ml LPS (Sigma), 25nM Rapamycin (Calbiochem), 10 mM N-Acetyl-L-cysteine (Sigma).

In vivo CD40 stimulation

Mice were i.p injected with 250 μg functional grade purified anti-CD40 (1C10) or corresponding rat IgG2a isotype control (eBioscience) on d0. To analyze B cell proliferation mice were i.p. injected with 2 mg BrdU (in PBS) on day 3 and sacrificed 2 h later. Cells that have incorporated BrdU were detected using the BrdU Flow Kit according to manufacturer's instructions (BD Biosciences).

Metabolic Assays

Glucose consumption and lactate production were measured in cell supernatants obtained at day 3 of culture using the YSI 2950 metabolite analyzer (YSI Life Sciences). The Seahorse XF24 metabolite analyzer was used to measure oxygen consumption and proton production. $CD43^-$ B cells were cultured over night with the indicated stimulations, counted and 1×10^6 cells (anti-CD40+IL-4–stimulated cells) or 2×10^6 cells (anti-IgM stimulated cells) were plated on Cell-Tak (BD Biosciences) coated Seahorse cell culture plates. Cells were incubated for 1.5h in Seahorse assay medium supplemented with 10 mM glucose and 1 mM Sodium pyruvate before measurement. The Seahorse BioScience XF Cell Mito Stress Test kit was used to examine different parameters of respiration, basal respiration, coupling efficiency and spare respiratory capacity. Experiments were performed at the Sanford Burnham Prebys Cancer Metabolism Core.

Glucose uptake

Glucose uptake *in vivo* was measured in naïve and germinal center B cells. To measure glucose uptake in germinal center B cells, mice were immunized with SRBC and i.v. injected with 100 μl 2 mM 2-(*N*-(7-Nitrobenz-2-oxa-1,3-diazol-4-yl)Amino)-2-Deoxyglucose (2NBDG, Cayman Chemical Company) on day 7. Mice were sacrificed 1 h after 2NBDG injection. 2NBDG uptake in different B cell populations was measured by flow cytometry.

2DG injection

Mice were immunized with SRBC (d0) and i.p. injected with 500 mg/kg 2DG (Sigma) on d4,5,6 and sacrificed on d7. Germinal center B cells were analyzed by flow cytometry.

Immunizations and antigen specific antibody detection

Mice were injected with tamoxifen on three subsequent days and immunized with 100 μl packed SRBCs (Colorado Serum Company). Mice were sacrificed 7 days later. Spleens were analyzed for the presence of germinal centers by flow cytometry and histology. SRBC-

specific IgM and IgG1 titers were measured in sera from day 0 and day 8 by flow cytometry. SRBC were incubated for 20 min on ice with different concentrations of the serum sample, washed with flow cytometry buffer and stained with anti-mouse IgM and anti-mouse IgG1. Mean fluorescence intensities of the SRBCs bound anti-IgM and anti-IgG1 antibodies were plottet against the dilutions, values in the linear range were used for the final presentation of the results. To study GC proliferation and survival after acute GSK3 deletion, mice were first immunized with SRBCs, injected with tamoxifen on three subsequent days and sacrificed as indicated in the respective figure legend. To analyze apoptosis induction, splenic cells were stained with B220 (RA3-6B2, eBioscience), GL7 (eBioscience) and Fas (Jo2, BD Pharmingen) to identify GC B cells and with Annexin V using the Annexin V detection kit (BD Biosciences). To study affinity maturation mice were injected with tamoxifen on three subsequent days, rested for two days and immunized with 100 μg alum precipitated NP_{25}-KLH (Biosearch Technologies). Serum was collected on d0, d7 and d14. Antibody titers were determined by ELISA. NP_4-BSA and NP_{23}-BSA coated plates were used to detect high affinity antibodies and total titers, respectively.

Histology

Spleens were embedded in Tissue Tek O.C.T (Sakura Finetek) and frozen at –80°C. Sections were fixed with acetone, blocked with PBS+5% FBS for 1 h at 19–25 °C and stained with a combination of various antibodies: Peanut agglutinin (Vector Labs), B220 (RA3-6B2, eBioscience), Metallophilic Macrophages -1 (Moma-1, Abcam), IgM (II/41, eBioscience), CD5 (53-7.3, eBioscience), CD35 (8C12, BD Pharmingen), CD3e (145-2C11) for 2 h at 19–25 °C. Streptavidin Cy3 (Jackson) was used in a second step to detect biotinylated antibodies. Sections were washed 3 times in between every step with PBS+0.5% Tween. Images were acquired on a Zeiss Axio ImagerM1 Microscope (Zeiss) using SlideBook software (Intelligent Imaging Innovations) at 19–25 °C with EC Plan-NEOFLUAR objectives (Zeiss).

Detection of hypoxic regions in the spleen

Mice were immunized with SRBCs and i.p. injected with 60 μg/g Hypoxyprobe-1 (Hypoxyprobe) and sacrificed by cervical dislocation 1 h later. Frozen spleen sections were prepared. An APC-labeled mouse monoclonal antibody detecting pimonidazole adducts (Hypoxyprobe Red APC kit, Hypoxyprobe) was used to visualize hypoxic cells.

Immunoblotting

Cells were lysed in RIPA buffer, immunoblotting was performed following standard procedures. The following antibodies were obtained from Cell Signaling: Cyclin D3 (DCS22), MEK1/2 (DIA5), GSK3 (D75D3), β-Catenin (polyclonal, Lot 3), c-Myc (D84C12), p27 Kip1 (polyclonal, Lot 5), phospho-p70 S6 Kinase T389 (108D2), phospho-S6 S235/236 (D57.2.2E). A horseradish peroxidase coupled goat anti-rabbit antibody (Jackson) was used as a secondary antibody. 1% ovalbumin in PBS + 0.1% Tween20 was used as blocking buffer.

Generation of induced germinal center B cells

Induced germinal center B cells were generated by culturing B cells on the feeder cell line CD40LB[24] in the presence of IL-4 for 5 days.

Software and Statistical Analysis

Gimp (GNU Image Manipulation Program) and GraphPad Prism (GraphPad Software) were used for image editing and statistical analysis, respectively. The presented western blots were cropped for clarity. The viSNE algorithm was used to visualize data obtained from mass cytometry. Statistical significance of observed differences was evaluated as indicated in the figure legends. Significant differences between the control and the experimental group are marked with and asterisk. Obtained *P*-values are indicated in the figure legend. Unless stated otherwise, statistical data are shown as mean values. In graphs showing data as dot plots each symbol represents a biological replicate (an individual mouse or a cell culture sample originating from an individual mouse). Statistical tests used are specified in the respective figure legend.

Data availability

The data that support the findings of this study are available from the corresponding author upon request.

Supplementary Material

Refer to Web version on PubMed Central for supplementary material.

Acknowledgments

References

1. Victora GD, et al. Germinal center dynamics revealed by multiphoton microscopy with a photoactivatable fluorescent reporter. Cell. 2010; 143:592–605. [PubMed: 21074050]

2. Calado DP, et al. The cell-cycle regulator c-Myc is essential for the formation and maintenance of germinal centers. Nat Immunol. 2012; 13

3. Dominguez-Sola D, et al. The proto-oncogene MYC is required for selection in the germinal center and cyclic reentry. Nat Immunol. 2012; 13:1083–1091. [PubMed: 23001145]

4. Doughty CA, et al. Antigen receptor-mediated changes in glucose metabolism in B lymphocytes: role of phosphatidylinositol 3-kinase signaling in the glycolytic control of growth. Blood. 2006; 107:4458–4465. [PubMed: 16449529]

5. Woodland RT, et al. Multiple signaling pathways promote B lymphocyte stimulator dependent B-cell growth and survival. Blood. 2008; 111:750–760. [PubMed: 17942753]

6. Dufort FJ, et al. Cutting edge: IL-4-mediated protection of primary B lymphocytes from apoptosis via Stat6-dependent regulation of glycolytic metabolism. J Immunol. 2007; 179:4953–4957. [PubMed: 17911579]

7. Beurel E, Grieco SF, Jope RS. Glycogen synthase kinase-3 (GSK3): regulation, actions, and diseases. Pharmacol Ther. 2015; 148:114–131. [PubMed: 25435019]

8. Sutherland C. What Are the bona fide GSK3 Substrates? Int J Alzheimers Dis. 2011; 2011:505607. [PubMed: 21629754]

9. McNeill H, Woodgett JR. When pathways collide: collaboration and connivance among signalling proteins in development. Nat Rev Mol Cell Biol. 2010; 11:404–413. [PubMed: 20461097]

10. Cross DA, Alessi DR, Cohen P, Andjelkovich M, Hemmings BA. Inhibition of glycogen synthase kinase-3 by insulin mediated by protein kinase B. Nature. 1995; 378:785–789. [PubMed: 8524413]

11. Fang X, et al. Phosphorylation and inactivation of glycogen synthase kinase 3 by protein kinase A. Proc Natl Acad Sci U S A. 2000; 97:11960–11965. [PubMed: 11035810]

12. Sutherland C, Leighton IA, Cohen P. Inactivation of glycogen synthase kinase-3 beta by phosphorylation: new kinase connections in insulin and growth-factor signalling. Biochem J. 1993; 296(Pt 1):15–19. [PubMed: 8250835]

13. Zhao Y, et al. Glycogen synthase kinase 3alpha and 3beta mediate a glucose-sensitive antiapoptotic signaling pathway to stabilize Mcl-1. Mol Cell Biol. 2007; 27:4328–4339. [PubMed: 17371841]

14. Jacobs KM, et al. GSK-3beta: A Bifunctional Role in Cell Death Pathways. International journal of cell biology. 2012; 2012:930710. [PubMed: 22675363]

15. Cato MH, Chintalapati SK, Yau IW, Omori SA, Rickert RC. Cyclin D3 is selectively required for proliferative expansion of germinal center B cells. Mol Cell Biol. 2011; 31:127–137. [PubMed: 20956554]

16. Semenza GL, Roth PH, Fang HM, Wang GL. Transcriptional regulation of genes encoding glycolytic enzymes by hypoxia-inducible factor 1. J Biol Chem. 1994; 269:23757–23763. [PubMed: 8089148]

17. Rickert RC. New insights into pre-BCR and BCR signalling with relevance to B cell malignancies. Nat Rev Immunol. 2013; 13:578–591. [PubMed: 23883968]

18. Amir el AD, et al. viSNE enables visualization of high dimensional single-cell data and reveals phenotypic heterogeneity of leukemia. Nat Biotechnol. 2013; 31:545–552. [PubMed: 23685480]

19. Doble BW, Patel S, Wood GA, Kockeritz LK, Woodgett JR. Functional redundancy of GSK-3alpha and GSK-3beta in Wnt/beta-catenin signaling shown by using an allelic series of embryonic stem cell lines. Dev Cell. 2007; 12:957–971. [PubMed: 17543867]

20. Rickert RC, Roes J, Rajewsky K. B lymphocyte-specific, Cre-mediated mutagenesis in mice. Nucleic Acids Res. 1997; 25:1317–1318. [PubMed: 9092650]

21. Khalil AM, Cambier JC, Shlomchik MJ. B cell receptor signal transduction in the GC is short-circuited by high phosphatase activity. Science. 2012; 336:1178–1181. [PubMed: 22555432]

22. Srinivas S, et al. Cre reporter strains produced by targeted insertion of EYFP and ECFP into the ROSA26 locus. BMC Dev Biol. 2001; 1:4. [PubMed: 11299042]

23. Forster I, Rajewsky K. The bulk of the peripheral B-cell pool in mice is stable and not rapidly renewed from the bone marrow. Proc Natl Acad Sci U S A. 1990; 87:4781–4784. [PubMed: 2352948]

24. Nojima T, et al. In-vitro derived germinal centre B cells differentially generate memory B or plasma cells in vivo. Nat Commun. 2011; 2:465. [PubMed: 21897376]

25. Sengupta S, Peterson TR, Sabatini DM. Regulation of the mTOR complex 1 pathway by nutrients, growth factors, and stress. Mol Cell. 2010; 40:310–322. [PubMed: 20965424]

26. Gregory MA, Qi Y, Hann SR. Phosphorylation by glycogen synthase kinase-3 controls c-myc proteolysis and subnuclear localization. J Biol Chem. 2003; 278:51606–51612. [PubMed: 14563837]

27. Sander S, et al. Synergy between PI3K signaling and MYC in Burkitt lymphomagenesis. Cancer Cell. 2012; 22:167–179. [PubMed: 22897848]

28. Hsieh AL, Walton ZE, Altman BJ, Stine ZE, Dang CV. MYC and metabolism on the path to cancer. Seminars in Cell & Developmental Biology. 2015; 43:11–21. [PubMed: 26277543]

29. Marchi S, et al. Mitochondria-ros crosstalk in the control of cell death and aging. Journal of signal transduction. 2012; 2012:329635. [PubMed: 22175013]

30. Cho SH, et al. Germinal centre hypoxia and regulation of antibody qualities by a hypoxia response system. Nature. 2016; 537:234–238. [PubMed: 27501247]

31. Abbott RK, et al. Germinal Center Hypoxia Potentiates Immunoglobulin Class Switch Recombination. J Immunol. 2016; 197:4014–4020. [PubMed: 27798169]

32. Caro-Maldonado A, et al. Metabolic reprogramming is required for antibody production that is suppressed in anergic but exaggerated in chronically BAFF-exposed B cells. J Immunol. 2014; 192:3626–3636. [PubMed: 24616478]

33. Dang CV, Kim JW, Gao P, Yustein J. Hypoxia and metabolism - Opinion - The interplay between MYC and HIF in cancer. Nature Reviews Cancer. 2008; 8:51–56. [PubMed: 18046334]

34. Zhang H, et al. HIF-1 inhibits mitochondrial biogenesis and cellular respiration in VHL-deficient renal cell carcinoma by repression of C-MYC activity. Cancer Cell. 2007; 11:407–420. [PubMed: 17482131]

35. Inoki K, et al. TSC2 integrates Wnt and energy signals via a coordinated phosphorylation by AMPK and GSK3 to regulate cell growth. Cell. 2006; 126:955–968. [PubMed: 16959574]

36. Azoulay-Alfaguter I, Elya R, Avrahami L, Katz A, Eldar-Finkelman H. Combined regulation of mTORC1 and lysosomal acidification by GSK-3 suppresses autophagy and contributes to cancer cell growth. Oncogene. 2015; 34:4613–4623. [PubMed: 25500539]

37. Stretton C, et al. GSK3-mediated raptor phosphorylation supports amino-acid-dependent mTORC1-directed signalling. Biochem J. 2015; 470:207–221. [PubMed: 26348909]
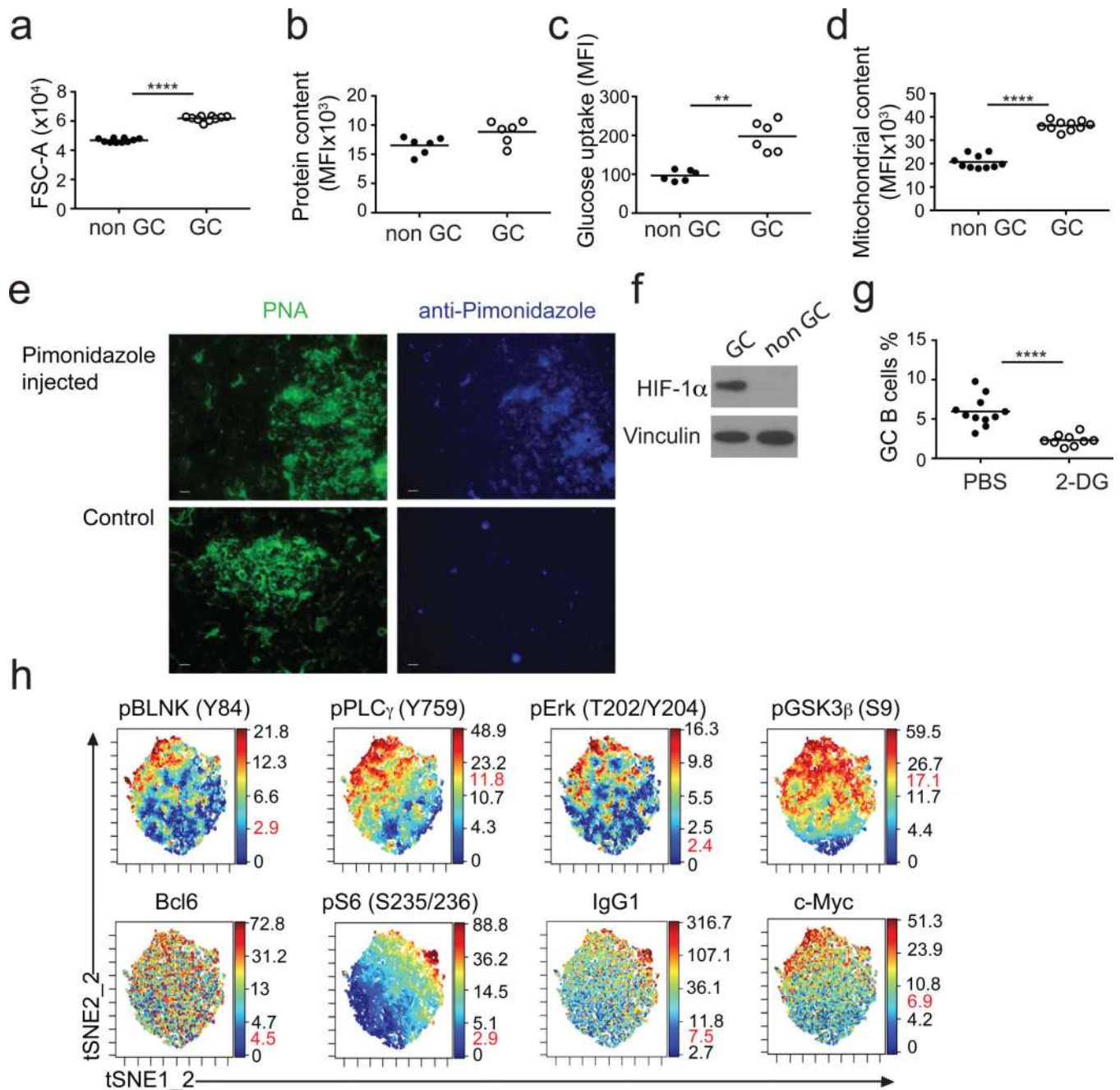
**Figure 1. GC B cells face increased metabolic demands**

(a) Cell size (FSC-A) of freshly isolated GC B cells (n=10) (B220$^+$, Fas$^+$, GL7$^+$) and non-GC B cells (n=10) (B220$^+$, Fas$^-$, GL7$^-$). Significance (****p<0.0001) was determined using the Mann-Whitney test (b) Protein levels of GC B cells (n=6) (B220$^+$, Fas$^+$, GL7$^+$) and non-GC B cells (n=6) (B220$^+$, Fas$^-$, GL7$^-$) B cells. Significance (p=0.06) was determined using the Mann-Whitney test (c) Mice were immunized with SRBC and i.v.-injected with 2NBDG 7 days later. 2NBDG uptake was measured by flow cytometry. The obtained MFIs from GC B cells (n=6) (B220$^+$, Fas$^+$, GL7$^+$) and non-GC B cells (n=6) (B220$^+$, Fas$^-$, GL7$^-$) are shown. Significance (**p=0.002) was determined using the Mann-Whitney test (d)

Mitochondrial mass as determined by MitoTracker Red CMX Ros labeling of GC and non GC B cells. Significance (****p<0.0001) was determined using the Mann-Whitney test **(e)** Detection of hypoxic regions in the spleen from SRBC immunized mice. Results are representative for 3 mice. Scale bar shows 10 µ1. **(f)** Hif-1α expression in lysates from purified GC B cells (Fas⁺, GL7⁺, B220⁺, CD11c⁻, CD43⁻, IgD⁻) and non-GC B cells (Fas⁺, GL7⁺, B220⁺, CD11c⁻, CD43⁻, GL7⁻). Results are representative of 4 sets of samples. **(g)** Mice were immunized with SRBC, injected with PBS (n=11) or 2DG (n=9) on day 4,5,6 and sacrificed on day 7. The percentage of GC B cells (B220⁺, Fas⁺, GL7⁺) in the spleen is shown. Significance (****p<0.0001) was determined using the t-test with Welch's correction. **(h)** Phosphorylation and expression of the indicated molecules in GC B cells (B220⁺, CD19⁺, GL7⁺, Fas⁺) was analyzed by CyTOF Mass Cytometry. Numbers highlighted in red show mean values obtained from non-GC B cells. Data are displayed using the t-Distributed Stochastic Neighbor Embedding (tSNE) algorithm. P-BLNK, p-GSK3, p-Erk, pS6 and p- PLCγ2 levels were used as sorting parameters. Plots are representative of 4 independent experiments. All experiments were performed using wildtype mice. Mice were sacrificed 7 days after immunization.
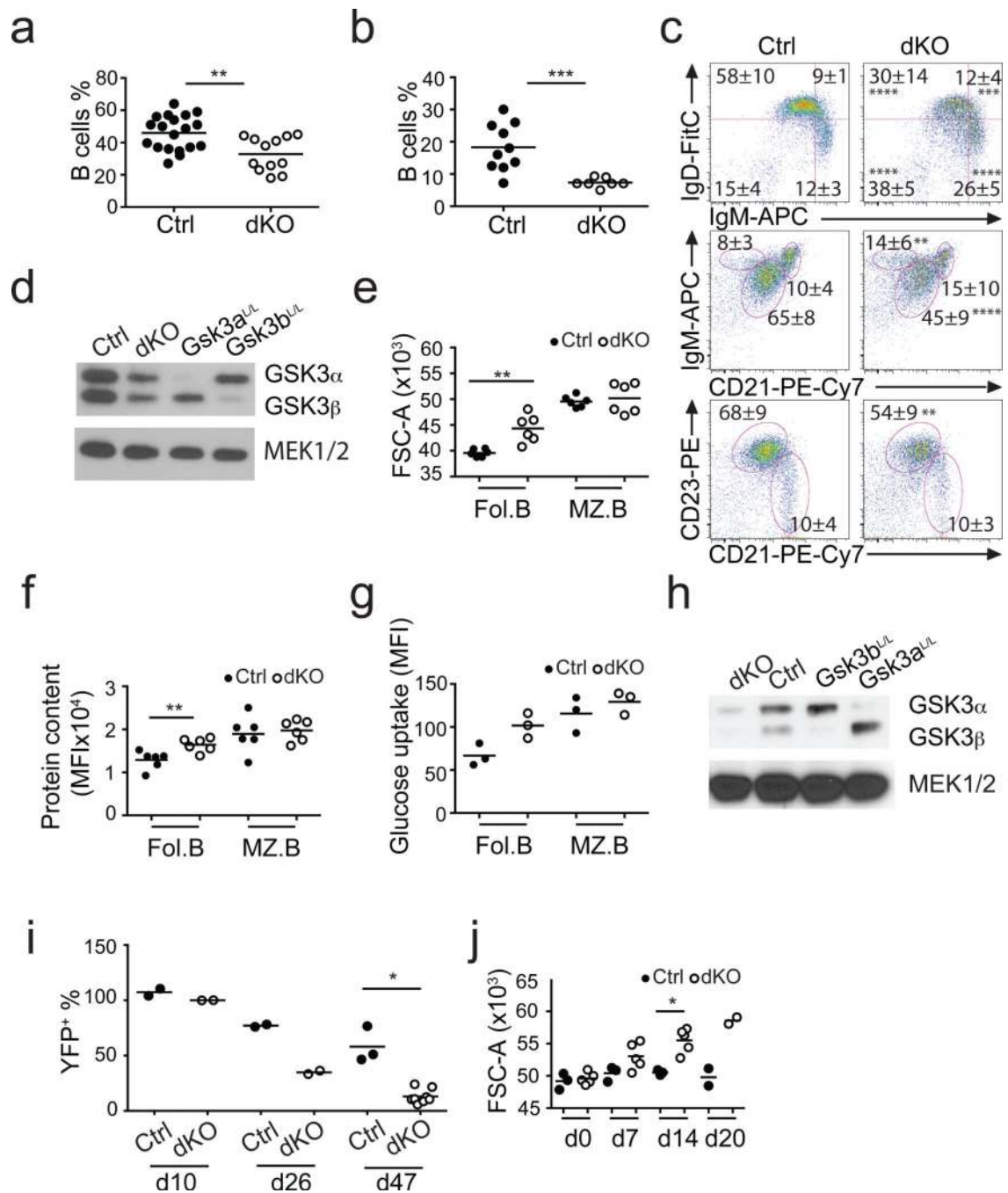
Figure 2. GSK3 promotes B cell quiescence and homeostasis

(a+b) Graph shows the frequency of B cells (B220[+]) in the spleen (n=19 WT, 12 dKO) (a) and peripheral lymph nodes (n=10 WT, n=7 dKO) (b). Significance (for spleen **p=0.0021, for LN ***p=0.004) was determined using the t test and the Mann-Whitney test respectively. (c) Analysis of B cell maturation in the spleen. Displayed cells are pre-gated based on B220 expression. Plots are representative of >9 mice. Significance was determined using the t test (for values presented in the upper and middle panel) and the Mann-Whitney test (for values in the bottom panel) (**** p < 0.0001, ***p<0.001, **p<0.01) Mice used: *Gsk3a*^{+/+} x

Gsk3b$^{+/+}$ *x Cd19*^{Cre} (Ctrl) and *Gsk3a*$^{L/L}$ x *Gsk3b*$^{L/L}$ *x Cd19*^{Cre} (dKO). **(d)** GSK3 protein expression in lysates from splenic B cells isolated from *Gsk3a*$^{+/+}$ x *Gsk3b*$^{+/+}$ *x Cd19*^{Cre} (Ctrl), *Gsk3a*$^{L/L}$ x *Gsk3b*$^{+/+}$ *x Cd19*^{Cre} (Gsk3a$^{L/L}$), *Gsk3a*$^{+/+}$ x *Gsk3b*$^{L/L}$ *x Cd19*^{Cre} (Gsk3b$^{L/L}$) and *Gsk3a*$^{L/L}$ x *Gsk3b*$^{L/L}$ *x Cd19*^{Cre} (dKO) mice. MEK1/2 was used as loading control. Shown western blot is representative for 4 experiments. **(e)** Forward scatter (FSC-A) values as a measure of cell size in freshly isolated follicular (n=6) (B220$^+$, CD23$^+$, CD21^{lo}) and marginal zone (n=6) (B220$^+$, CD23$^-$, CD21^{hi}) B cells from *Gsk3a*$^{+/+}$ x *Gsk3b*$^{+/+}$ *x Cd19*^{Cre} (Ctrl), *Gsk3a*$^{L/L}$ x *Gsk3b*$^{L/L}$ *x Cd19*^{Cre} (dKO) mice. Significance (**p=0.002) was determined using the Mann-Whitney test. **(f)** Protein levels of follicular (n=6) (B220$^+$, CD23$^+$, CD21^{lo}) and marginal zone (n=6) (B220$^+$, CD23$^-$, CD21^{hi}) B cells from *Gsk3a*$^{+/+}$ x *Gsk3b*$^{+/+}$ *x Cd19*^{Cre} (Ctrl), *Gsk3a*$^{L/L}$ x *Gsk3b*$^{L/L}$ *x Cd19*^{Cre} (dKO) mice. Significance (**p=0.0043) was determined using the Mann-Whitney test. **(g)** Glucose uptake by follicular B cells (n=3) and marginal zone (n=3) B cells from *Gsk3a*$^{+/+}$ x *Gsk3b*$^{+/+}$ *x Cd19*^{Cre} (Ctrl), *Gsk3a*$^{L/L}$ x *Gsk3b*$^{L/L}$ *x Cd19*^{Cre} (dKO) mice injected with 2NBDG and analyzed 1h later by flow cytometry. One of two experiments with a total of 6 mice per genotype is shown. **(h)** Immunoblots for GSK3 protein from splenic B cells isolated from *Gsk3a*$^{+/+}$ x *Gsk3b*$^{+/+}$ *x hCd20- Tam*^{Cre} (Ctrl), *Gsk3a*$^{L/L}$ x *Gsk3b*$^{+/+}$ *x hCd20-Tam*^{Cre} (Gsk3a$^{L/L}$), *Gsk3a*$^{+/+}$ x *Gsk3b*$^{L/L}$ *x hCd20-Tam*^{Cre} (Gsk3b$^{L/L}$) and *Gsk3a*$^{L/L}$ x *Gsk3b*$^{L/L}$ *x hCd20-Tam*^{Cre} (dKO) mice. Mice were injected with tamoxifen on 3 subsequent days and analyzed 8 days after the last injection. MEK1/2 was used as loading control. **(i)** Relative frequency of YFP$^+$ splenic follicular B cells from *Gsk3a*$^{+/+}$ x *Gsk3b*$^{+/+}$ *x hCd20- Tam*^{Cre} (Ctrl) and *Gsk3a*$^{L/L}$ x *Gsk3b*$^{L/L}$ *x hCd20-Tam*^{Cre} (dKO) mice 10, 26 and 47 days after tamoxifen injection. The measured frequency of YFP$^+$ cells was normalized to the value obtained in the blood at the peak of induction (d7). Significance (*p=0.0121) was determined using the Mann-Whitney test. **(j)** FSC-A values of YFP$^+$ B cells from the blood of *Gsk3a*$^{+/+}$ x *Gsk3b*$^{+/+}$ *x hCd20- Tam*^{Cre} (Ctrl) and *Gsk3a*$^{L/L}$ x *Gsk3b*$^{L/L}$ *x hCd20-Tam*^{Cre} (dKO) mice at day 0, 7, 14 and 20 after tamoxifen injection. Significance (*p=0.0357) was determined using the Mann-Whitney test.
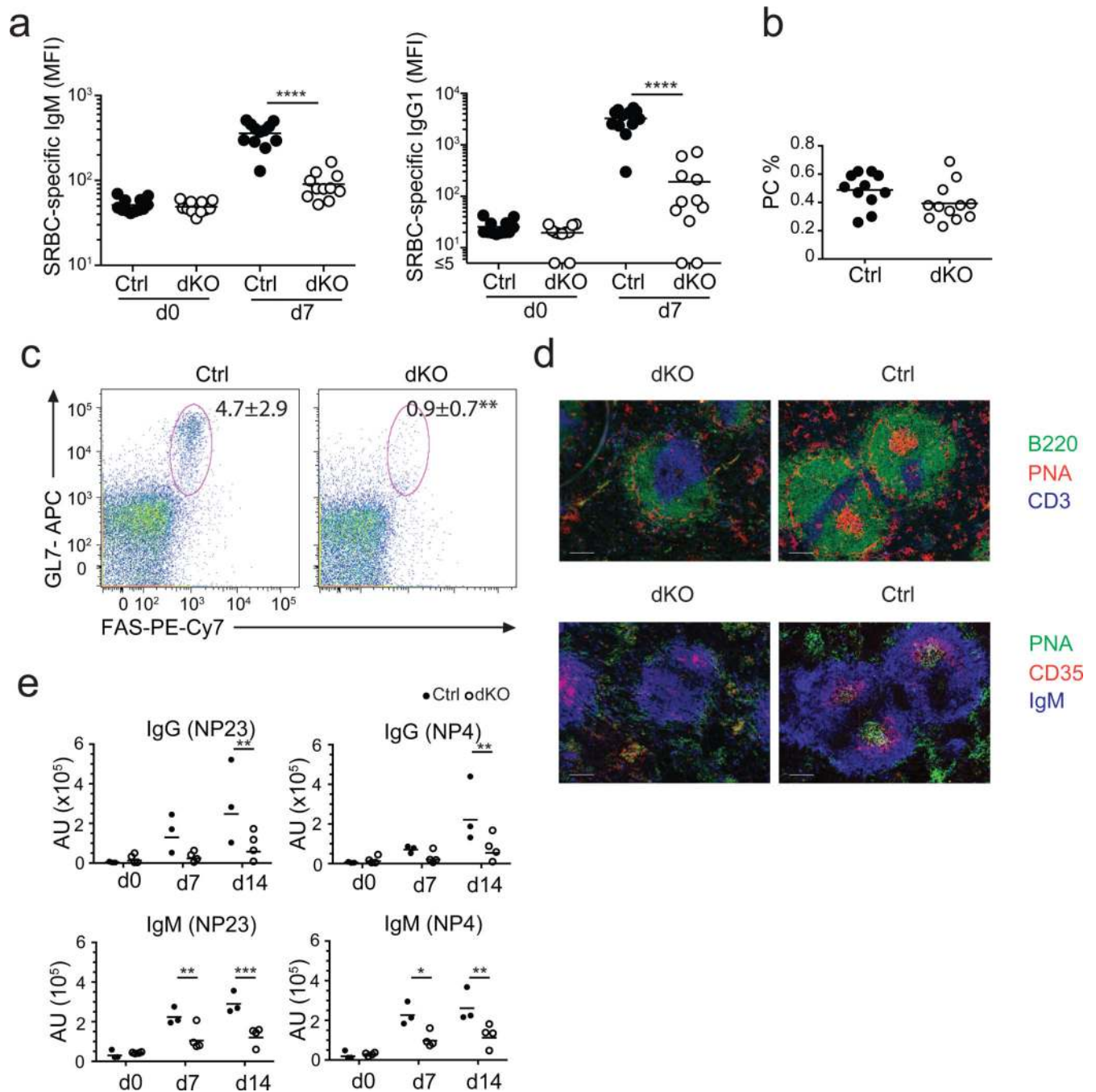
Figure 3. GSK3 is required for T cell-dependent B cell responses

(a) Serum levels of SRBC-specific IgM (left) and IgG1 (right) antibody on d0 and d7 as measured by flow cytometric staining (WT n=11, dKO n=12). Plots show the obtained mean fluorescence intensities. Significance (****p<0.0001) was determined using the t test with Welch's correction (for IgM) and the Mann-Whitney test (for IgG1). **(b)** The relative frequency of plasma cells (CD138+, B220lo) in the spleen 7 days after SRBC immunization is shown. **(c)** Dot plots of GC B cells 7 days after immunization with SRBC. Plots are representative of 11 WT and 12 dKO mice. Significance (**p=0.0013) was determined using

the t test with Welch's correction **(d)** Analysis of frozen spleen sections 7days after SRBC immunization. Scale bar shows μ1. Images are representative of two mice per genotype analyzed. **(e)** Serum titers of high affinity (NP_4) and total (NP_{23}) IgM and IgG at days 0, 7 and 14 following NP-KLH immunization. Mice shown: *Gsk3a*$^{+/+}$ x *Gsk3b*$^{+/+}$ *x hCd20-Tam*^{Cre} or *Gsk3a*$^{L/L}$ x *Gsk3b*$^{L/L}$ *x hCd20-Tam*$^{Cre-}$ (Ctrl) *Gsk3a*$^{L/L}$ x *Gsk3b*$^{L/L}$ *x hCd20-Tam*^{Cre} (dKO). Significance was determined using the two-way ANOVA test.
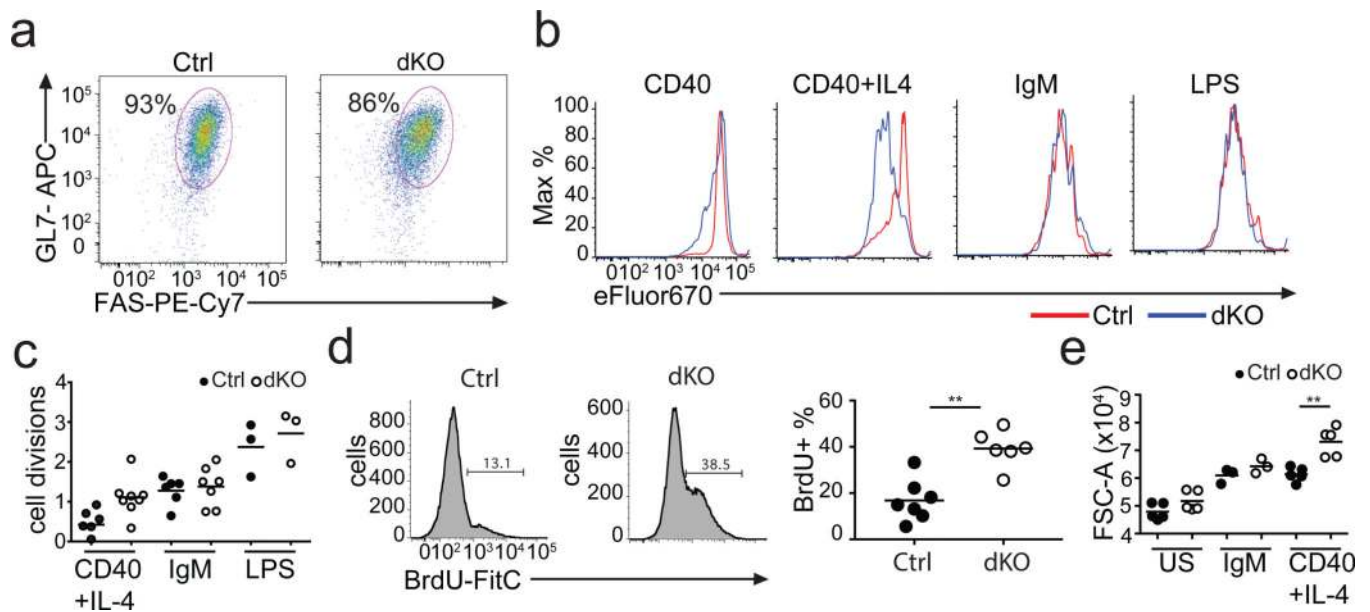
Figure 4. GSK3 inhibits CD40-induced B cell proliferation

(a) Induced germinal center B cells (iGB) were generated from Ctrl and dKO B cells using the feeder cell line CD40LB and exogenous IL-4. GL7 and Fas expression on iGB cells is shown. Plots are representative of 3 mice per genotype. **(b)** Histograms show B cell proliferation and **(c)** average number of cell divisions of Ctrl and dKO after 3 days of cell culture with the indicated stimuli. Mean values obtained from 3–7 experiments are shown. Significance (**p=0.0093) was determined using the Mann-Whitney test. **(d)** Mice were injected with anti-CD40, B cell proliferation was measured by BrdU incorporation 3 days later. Histograms show representative BrdU staining, the dot plot summarized the results from two independent experiments. Significance (**p=0.0043) was determined using the Mann-Whitney test. **(e)** FSC-A values of B cells from Ctrl and dKO mice cultured overnight with the indicated stimulations. Significance (**p=0.0079) was determined using the Mann-Whitney test.. Mice shown in a,b,c and e: $Gsk3a^{+/+}$ x $Gsk3b^{+/+}$ x $hCd20\text{-}Tam^{Cre}$ or $Gsk3a^{L/L}$ x $Gsk3b^{L/L}$ x $hCd20\text{-}Tam^{Cre-}$ (Ctrl) $Gsk3a^{L/L}$ x $Gsk3b^{L/L}$ x $hCd20\text{-}Tam^{Cre}$ (dKO). Mice shown in d: $Gsk3a^{+/+}$ x $Gsk3b^{+/+}$ x $Cd19^{Cre}$ or $Gsk3a^{L/L}$ x $Gsk3b^{L/L}$ x $Cd19^{Cre-}$ (Ctrl) $Gsk3a^{L/L}$ x $Gsk3b^{L/L}$ x $Cd19^{Cre}$ (dKO).
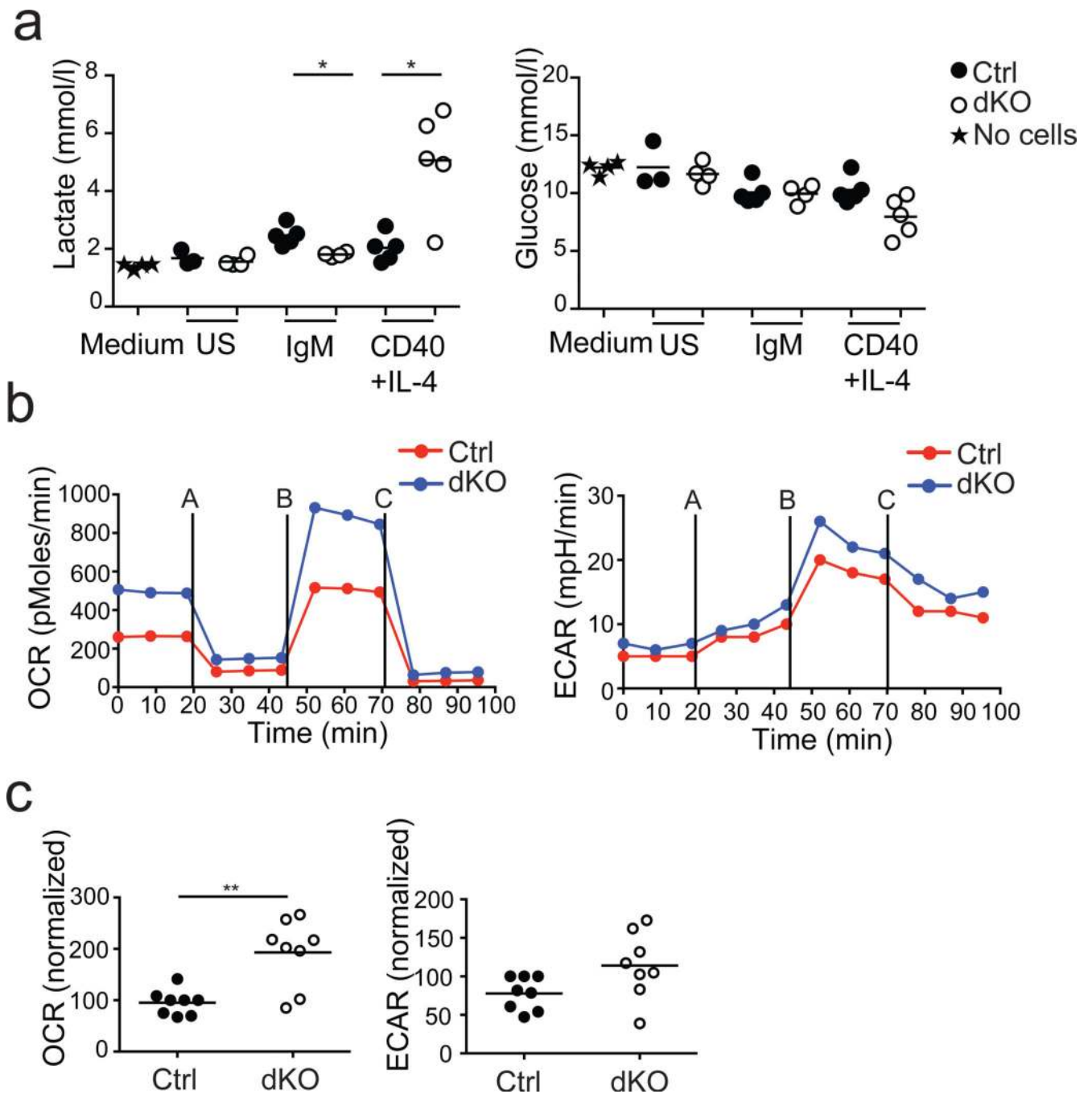
Figure 5. GSK3 limits CD40-induced metabolic activity

(a) Lactate and glucose concentrations in cell supernatants at day 3 of cell culture with the indicated stimuli is shown. B cells from tamoxifen-treated Ctrl and dKO mice were cultured at a concentration of 2×10^6 cells/ml. Values obtained from medium without cells are shown for reference. Significance (*p=0.0159) was determined using the Mann-Whitney test (b) Oxygen consumption (OCR) and extracellular acidification (ECAR) of B cells isolated from tamoxifen-treated Ctrl and dKO mice and stimulated over night with anti-CD40+IL-4 is shown. The following inhibitors were used: A= Oligomycin, B=FCCP, C=

Rotenone$^+$Antimycin. Graphs are representative of 8 mice per genotype. **(c)** Basal OCR and ECAR levels in B cells stimulated over night with anti-CD40$^+$IL-4 are shown. Graphs summarize data obtained from 3 independent experiments with 8 mice per genotype in total. In each experiment, values were normalized to a randomly chosen wildtype sample. Significance (**p=0.0036) was determined using the t test with the Welch's correction. Mice shown: *Gsk3a*$^{+/+}$ x *Gsk3b*$^{+/+}$ *x hCd20-Tam*^{Cre} or *Gsk3a*$^{L/L}$ x *Gsk3b*$^{L/L}$ *x hCd20-Tam*$^{Cre-}$ (Ctrl) *Gsk3a*$^{L/L}$ x *Gsk3b*$^{L/L}$ *x hCd20-Tam*^{Cre} (dKO).
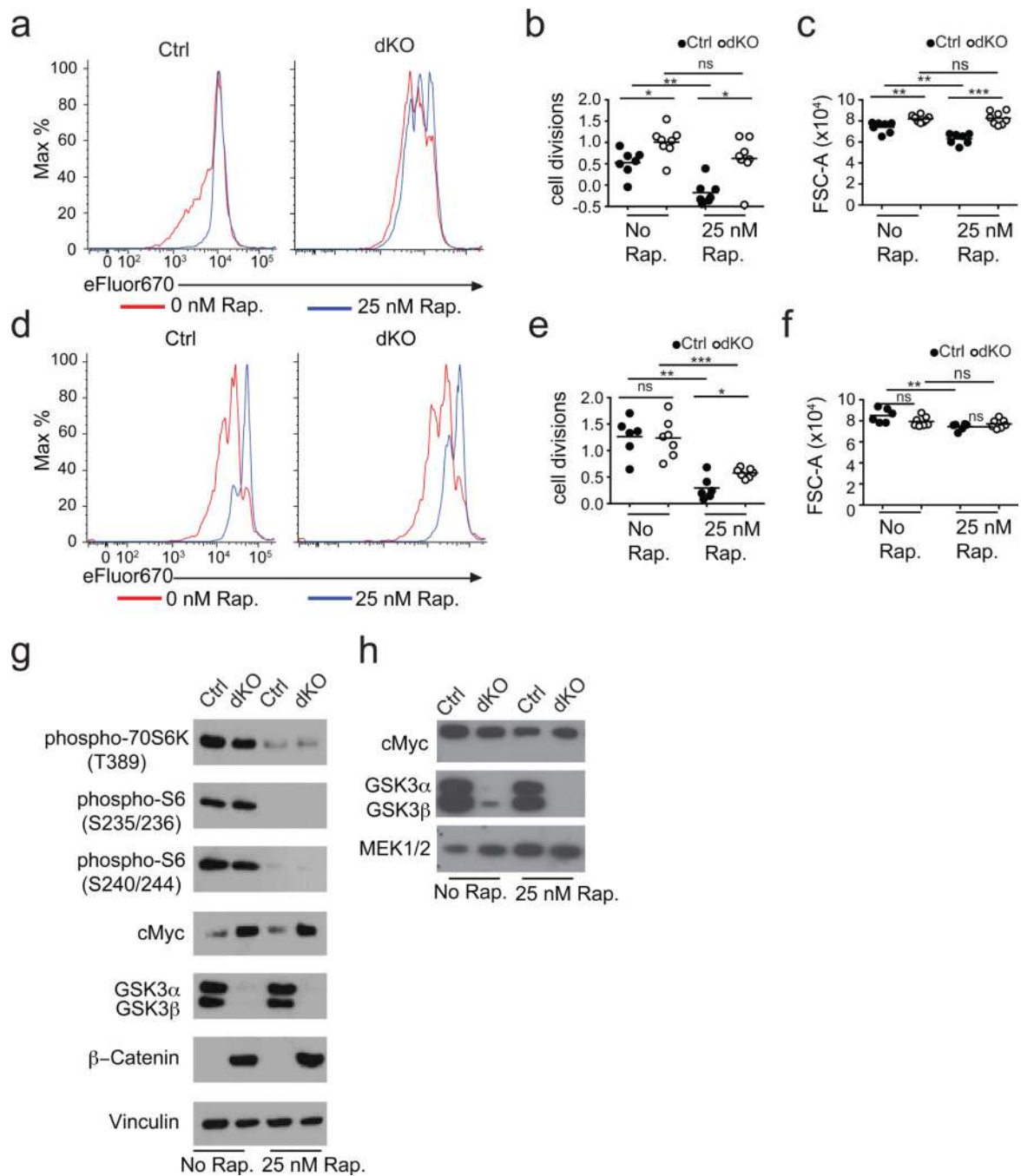
Figure 6. GSK3 promotes rapamycin sensitivity and c-Myc degradation
(**a**) Proliferation, (**b**) average number of cell divisions and (**c**) size (FSC-A) of Ctrl and dKO B cells after 3 days of cell culture with anti- CD40+IL-4 in the presence or absence of 25nM rapamycin. Significance (*p<0.05 **p=0.01,***p<0.001) was determined using the Mann Whitney test. (**d**) Proliferation, (**e**) average number of cell divisions and (**f**) size (FSC-A) of Ctrl and dKO B cells after 3 days of cell culture with anti-IgM in the presence or absence of 25nM rapamycin. Significance (**p=0.012 and 0.007 ***p=0.0003) was determined using the Mann Whitney test. (**g**) Cell lysates from Ctrl and dKO B cells stimulated with anti-
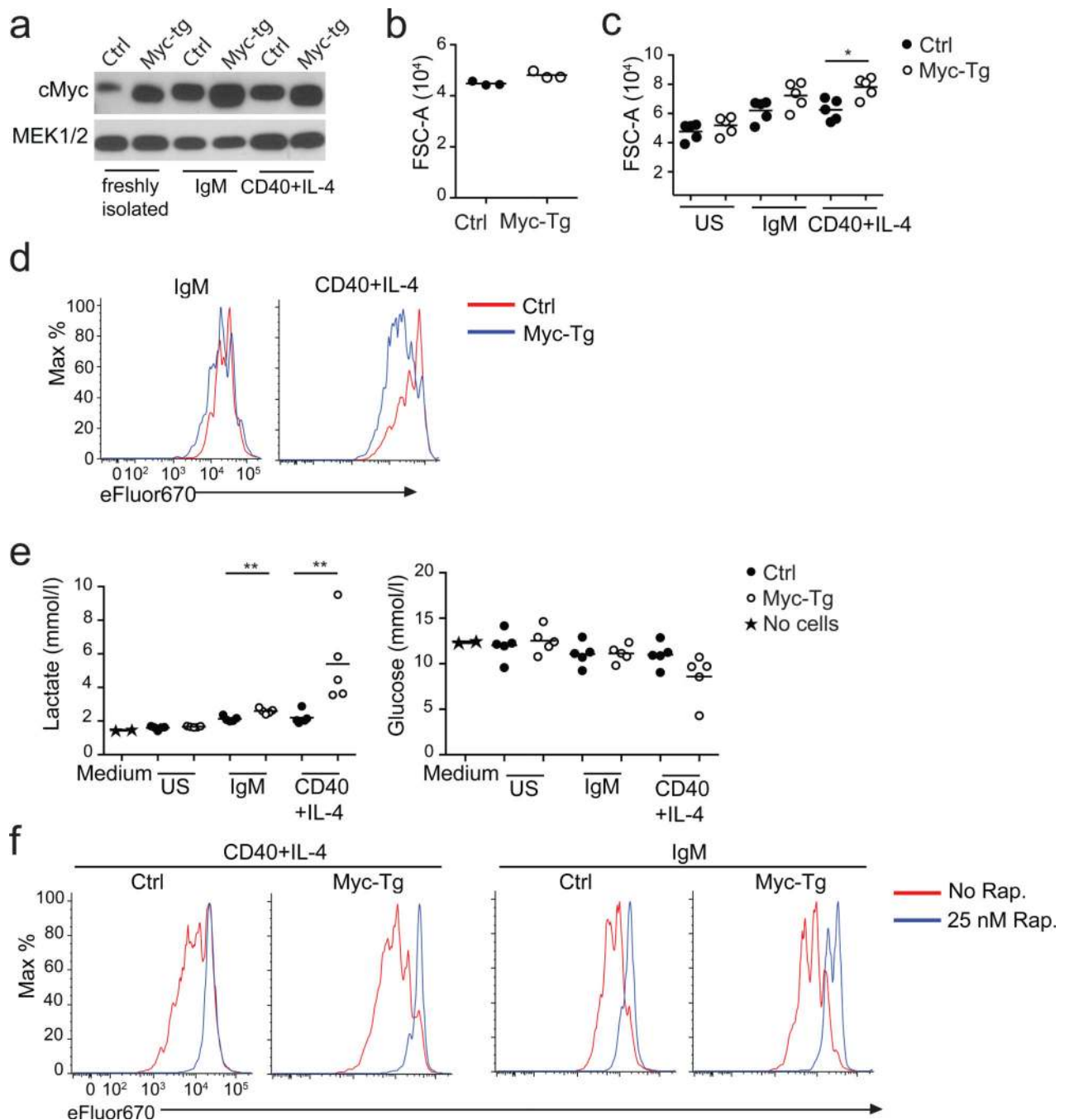
CD40$^+$IL-4 or **(h)** anti-IgM overnight in the presence or absence of 25nM rapamycin and probed for the indicated proteins. Results are representative of 3 independent experiments. Mice shown: *Gsk3a*$^{+/+}$ x *Gsk3b*$^{+/+}$ *x hCd20-Tam*^{Cre} or *Gsk3a*$^{L/L}$ x *Gsk3b*$^{L/L}$ *x hCd20-Tam*$^{Cre−}$ (Ctrl) *Gsk3a*$^{L/L}$ x *Gsk3b*$^{L/L}$ *x hCd20-Tam*^{Cre} (dKO). All mice were treated with tamoxifen on 3 consecutive days.

Figure 7. c-Myc as a functional target of GSK3

(a) Myc protein levels in freshly isolated, anti-IgM or anti- CD40^{+}IL-4 stimulated B cells from control and *Myc*-tg mice as determined by immunoblot. MEK1/2 was used as loading control. Results are representative of 3 independent experiments. **(b)** Cell size (FSC-A) of freshly isolated or **(c)** overnight cultured Ctrl and *Myc*-tg B cells. Significance (*p=0.0317) was determined using the Mann Whitney test. **(d)** Proliferation of Ctrl and *Myc*-tg B cells cultured for 3d with the indicated stimuli. Results are representative of 3 independent experiments. **(e)** Lactate (left) and glucose (right) concentration in cell supernatants at day 3
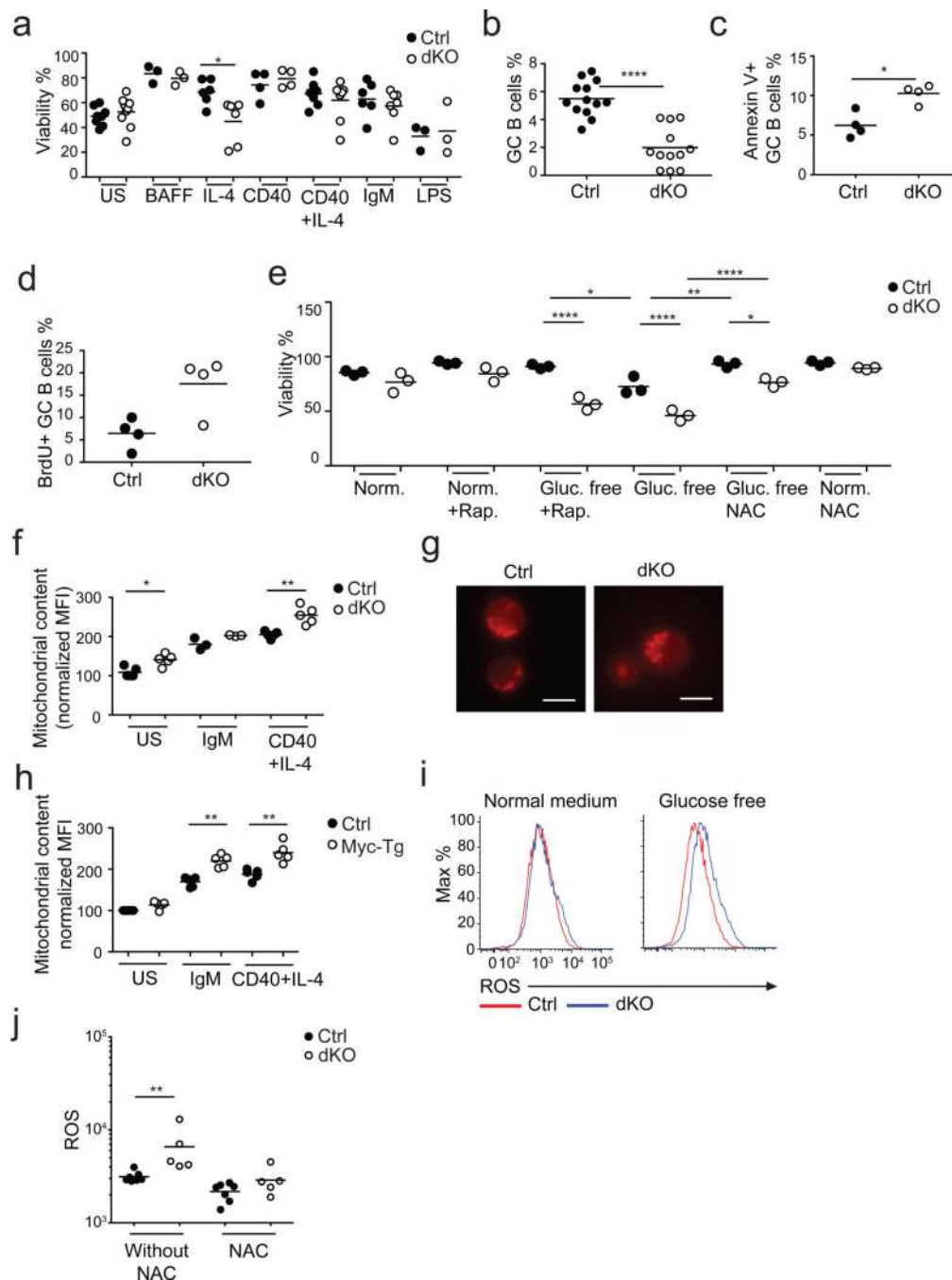
of cell culture with the indicated stimuli. Cells were cultured at a concentration of 1×10^6 cells/ml. Values obtained in medium without cells is shown for reference. Significance (**p=0.0079) was determined using the Mann Whitney test. **(f)** Proliferation of Ctrl and *Myc*-tg B cells cultured over for 3 days with the indicated stimuli in the presence or absence of 25 nM rapamycin. Results are representative of 3 independent experiments. Mice used: *R26Stop*^{FL}*Myc*×*Cd19*^{Cre} (Myc-Tg) and *Cd19*^{Cre} littermates (Ctrl).

Figure 8. GSK3 promotes B cell survival under glucose restriction
(a) Percent viable Ctrl and dKO B cells at day 3 of cell culture with the indicated stimuli. Significance (p=0.013) was determined using the Mann Whitney test. (b) Percent GC B cells in spleens from Ctrl (n=13) and dKO (n=12) mice immunized with SRBC on d0, injected with tamoxifen on day 6,7,8 and analyzed on day 10. Mice shown: *Gsk3a*^{+/+} x *Gsk3b*^{+/+} x *hCd20-Tam*[Cre] or *Gsk3a*[L/L] x *Gsk3b*[L/L] x *hCd20-Tam*[Cre−] (Ctrl) *Gsk3a*[L/L] x *Gsk3b*[L/L] x *hCd20-Tam*[Cre] (dKO). Significance (p<0.0001) was determined using the t test. (c) Percent Annexin V+ GC B cells in spleens from Ctrl (n=4) and dKO (n=4) mice immunized with

SRBC on d0, injected with tamoxifen on day 5,6,7 and analyzed on day 8. Mice shown: $Gsk3a^{L/L}$ x $Gsk3b^{L/L}$ x $hCd20\text{-}Tam^{Cre-}$ (Ctrl) $Gsk3a^{L/L}$ x $Gsk3b^{L/L}$ x $hCd20\text{-}Tam^{Cre}$ (dKO). Significance (*p=0.0286) was determined using the Mann Whitney test. **(d)** Percent BrdU$^+$ GC B cells in spleens from Ctrl (n=4) and dKO (n=4) mice immunized with SRBC on d0, injected with tamoxifen on day 5,6,7, injected with BrdU on day 9 and analyzed 3h later. Mice shown: $Gsk3a^{L/L}$ x $Gsk3b^{L/L}$ x $hCd20\text{-}Tam^{Cre-}$ (Ctrl) $Gsk3a^{L/L}$ x $Gsk3b^{L/L}$ x $hCd20\text{-}Tam^{Cre}$ (dKO).. Significance (p=0.0571) was determined using the Mann Whitney test. **(e)** Percent viable B cells from $Gsk3a^{+/+}$ x $Gsk3b^{+/+}$ x $hCd20\text{-}Tam^{Cre}$ or $Gsk3a^{L/L}$ x $Gsk3b^{L/L}$ x $hCd20\text{-}Tam^{Cre-}$ (Ctrl) $Gsk3a^{L/L}$ x $Gsk3b^{L/L}$ x $hCd20\text{-}Tam^{Cre}$ (dKO). mice isolated from tamoxifen-treated mice and cultured for 3 days in complete or glucose-free medium, in the presence of anti-CD40+IL4 with or without 25 nM rapamycin or with or without NAC. Graph depicts 3 independent experiments. Significance (*p<0.05, **p<0.01, ***p<0.001, ****p<0.0001) was determined using the ANOVA test with Tukey's correction for multiple comparisons. **(f)** Mitochondrial mass of $Gsk3a^{+/+}$ x $Gsk3b^{+/+}$ x $hCd20\text{-}Tam^{Cre}$ or $Gsk3a^{L/L}$ x $Gsk3b^{L/L}$ x $hCd20\text{-}Tam^{Cre-}$ (Ctrl) $Gsk3a^{L/L}$ x $Gsk3b^{L/L}$ x $hCd20\text{-}Tam^{Cre}$ (dKO).B cells isolated from tamoxifen-treated mice 10d after the last injection, cultured over night with the indicated stimuli. Significance (*p=0.0159, **p=0.0079) was determined using the Mann Whitney test. Values were from separate experiments were normalized to the value obtained from a randomly chosen unstimulated control sample. **(g)** Immunofluorescence of mitochondrial mass visualized by MitoTracker Red CMXRos staining in $Gsk3a^{+/+}$ x $Gsk3b^{+/+}$ x $hCd20\text{-}Tam^{Cre}$ (Ctrl) $Gsk3a^{L/L}$ x $Gsk3b^{L/L}$ x $hCd20\text{-}Tam^{Cre}$ (dKO). B cells stimulated with anti-CD40$^+$IL4 over night. **(h)** Mitochondrial mass was measured with by MitoTracker Red CMXRos labeling of Ctrl and *Myc*-tg B cells cultured over night with the indicated stimuli. Values were from separate experiments were normalized to the value obtained from unstimulated control cells. Significance (**p=0.0079) was determined using the Mann Whitney test. **(i)** ROS production in anti-CD40$^+$IL-4 stimulated $Gsk3a^{+/+}$ x $Gsk3b^{+/+}$ x $Cd19^{Cre}$ (Ctrl) and $Gsk3a^{L/L}$ x $Gsk3b^{L/L}$ x $Cd19^{Cre}$ (dKO) B cells cultured overnight in complete or glucose-free medium. Plots are representative for 3 independent experiments. **(j)** Freshly isolated splenic B cells from $Gsk3a^{L/L}$ x $Gsk3b^{L/L}$ x $Cd19^{Cre-}$ or $Gsk3a^{+/+}$ x $Gsk3b^{+/+}$ x $Cd19^{Cre}$ (Ctrl) and $Gsk3a^{L/L}$ x $Gsk3b^{L/L}$ x $Cd19^{Cre}$ (dKO) mice were stained for ROS production. As a control, samples were stained in parallel for ROS content in the presence of the ROS scavenger NAC. Significance (**p=0.0025) was determined using the Mann Whitney test.